Analysis of continuous spectral method for sampling stationary Gaussian random fields

Jocelyne Erhel, Mestapha Oumouni, Géraldine Pichot, Franck Schoefs

Analysis of continuous spectral method for sampling stationary Gaussian random fields

Jocelyne Erhel, Mestapha Oumouni, Géraldine Pichot, Franck Schoefs

November 24, 2018

Abstract

Problems of uncertainty quantification usually involve large number realizations of a stationary spatial Gaussian random field over a regular grid points. This paper analyzes the convergence of the continuous spectral method for generating a stationary Gaussian random field. The continuous spectral method is the classical approach which discretizes the spectral representation integral to construct an approximation of the field within the Fast Fourier Transform algorithm. The method can be used as an alternative of circulant embedding approach when the discrete covariance matrix is not valid. We demonstrate that the method is computationally attractive when the spectral is a smooth function and decreases rapidly to zero at infinity. In such case, The spectral method is a very versatile approach for generating Gaussian stochastic fields. A simulation results are realized using pseudo-random data based on Monte-Carlo simulations to illustrate the theoretical bound of the method regarding the regularity of the random field and its spectral density.

key words: Gaussian random field, Spectral simulation, spectral density, Fast Fourier Transform, Monte-Carlo simulation, Weak and strong error.

1 Introduction

In recent years, Problems of uncertainty quantification has attracted a lot of consideration in the scientific community. The common approach to deal with such uncertainties is to adopt a probabilistic framework by modelling parameters in the partial differential equations (PDE) with random fields. The computational aim is to estimate quantities of interest which are a functional of the outputs (solutions of PDE) of the model. (For example, moment and variance of the response of the model, higher order moments, probability of failure, or other statistics of the outputs).

In the material and structural engineering field, several material and geometrical properties (e.g., cover depth, diffusion coefficient, concrete strength, chloride external concentration, etc.) are expected to show considerable spatial uncertainty as a result of the effect of environmental aggressions, randomness of material composition and

the inconsistency of the workmanship [20, 16, 21]. For example, in the transport equation, the diffusion coefficient is classically modelled by a second-order stationary random function, to model highly spatial variations and to consider the limited knowledge of the material characteristics. A reasonable application is to model this coefficient as a log-normal distribution $\kappa = e^G$, where G is a Gaussian random field (GRF) defined by a suitable spectral density or a covariance model. The log-normal random field with exponential covariance is widely used in hydrogeology and groundwater flow simulations, to model the hydraulic conductivity (see, e.g., [2, 11, 14] and the references there). For such problems, Monte Carlo simulations are the most widely used approach to quantify the uncertainty in the output of the problems described by a partial differential equation. This method requires the generation of numerous realizations of the field G on a equidistant positions of the physical space. Such realizations of the Gaussian field can be performed by different approaches. The classical one to generate a stationary GRF is based on Cholesky factorization or the spectral decomposition (Discrete Karhunen Loève series expansion) of the covariance matrix. Even these decomposition is very simple, it involve a high cost of matrix factorizations since the classical algorithm for calculating such factorization has a computational cost of $O(N^3)$ flops.

The Circulant Embedding matrix approach [6, 7, 10, 22] has been developed to simulate a stationary GRF. This method is seen as a Factorization method in which the decomposition of a carefully chosen extension of the covariance matrix is performed by Discrete Fourrier Transform (DFT). It allows to generate a Gaussian vectors with exactly the target correlation structure. It seems that this method combines the best features of both the spectral and the matrix factorization to generate Gaussian vectors with exactly the target correlation structure via FFT. Nevertheless, the major disadvantages of such approach is that it requires the validity of the covariance matrix which implies that the Circulant Embedding matrix is non-negative definite. This sufficient condition will reached with a very large extension of the covariance matrix. In particular, for multi-dimensional simulations. Sometimes it yields to a truncated simulation for smooth fields (e.g. the Gaussian covariance function). In other cases of the covariance structure, the sufficient condition of non-negative definite matrix is almost not reached even with very large spatial extension (e.g. the sinus-cardinal covariance function).

Given the huge cost of such matrix decompositions, The continuous spectral method [5, 17, 18, 19] is very fast approach to simulate a stationary GRF. It can be seen as a trapezium rule of the spectral-integral representation [5, 17, 18, 19]. This yields to a simulation of a Gaussian random field which only approximates the desired statistics. The authors in [18, 17] expected that the precision of the method is of $O(\frac{1}{N})$ for a rough covariance model and with order $O(\frac{1}{N^2})$ for a smooth covariance function [19], where N is the number of the equidistant positions. Based on the accuracy of the quadrature approximation, authors in [13] provide error estimate of the method with order $O(\delta p)$ (for a strong error) where δp is the spacing size of the frequency domain. This latter is chosen as the inverse of double spatial length $\delta p = \frac{1}{2L}$ when we perform the quadrature by FFT. with additional assumption on the decay of the derivatives of the spectral density, they provide week error of $O((\delta p)^2)$. Further, both are not optimal since constants in the estimate bound decrease with

the length of the domain

The main framework of the present paper is to provide an optimal error bounds of the continuous spectral representation method which does not involves any kind of matrix decomposition [5, 17, 18, 19]. We provide bounds estimate for both strong and weak error of CSM. These estimates shows that the convergence of the method depends on the regularity and the decay rate of the spectral density. In general, these estimates bound are better than those given in [13, 18, 19, 17]. They show that the CSM is more attractive and efficient for widely class of spectral density model used in the practice in which the Gaussian random field and its spectral density are both smooth functions.

The paper is organized as follows. Section 2 recalls the concept and the proprieties of stationary GRF. Section 3 recalls the steps Spectral representation method for a complex simulation. Section 4, we derive estimates of weak and strong error estimate of the method. Finally, numerical illustrations are provided to illustrate the efficiency of the method.

2 Gaussian random field

In this section, we recall the definition and some properties of the Gaussian random field G. (Namely, a second order, stationary, isotropic, and ergodic field).

A random field is a sequence of random variable $(G(x,\cdot))_{x\in D}$ where the index x belongs in a given domain D on $\mathbb{R}^d$. Let $(\Omega, \mathcal{F}, dP)$ be a complete probability space and D in $\mathbb{R}^d$, then G is a measurable mapping $G : D \longrightarrow \Omega$. For a fixed $x \in D$, $G(x,\cdot)$ is a random variable on Ω.

Definition 2.1. *The field G is said to be a Gaussian field if for all linear combinations: $\sum_{j=1}^{N} \alpha_j G(x_j,\cdot)$ has a Gaussian distribution, for any choice of $\{x_1,\ldots,x_N\} \subset D$ and a real sequence $\alpha_1,\ldots,\alpha_N$.*

The random field is second-order if G has finite variance and for such field we can define its mean function $\mu := \mathbb{E}[G]$ and its covariance function:

$$Cov(x,y) := \mathbb{E}[(G(x,.)-\mu(x))(G(y,.)-\mu(y))], \quad x,y \in D.$$

The following result shows that a Gaussian random field is completely defined by its mean and its covariance function[23].

Theorem 2.1. *Let $Cov : D^2 \to \mathbb{R}$ be a symmetric and positive, i.e: Cov(x,y)=Cov(y,x) and $\sum_{i,j}^{N} Cov(x_i,y_j)a_i a_j^* \geq 0$ for $\{x_j\}_{j=0}^{N} \subset D$ and any complex sequence $\{a_j\}_{j=0}^{N} \subset \mathbb{C}$. Then there exist a Gaussian field G with zero mean and covariance function Cov.*

An important class of G are stationary and isotropic random fields

Definition 2.2. *The Gaussian field G is stationary if:*

$$\mu(x) = \mu \qquad and \qquad Cov(x,y) = C(x-y),$$

and we say that G is isotropic if Cov depends on the norm $r = \|x - y\|_2$,

$$Cov(x, y) = C(r).$$

A Gaussian field G with mean $\mathbb{E}[G(x)] = \mu(x)$ is said to be trend stationary if the centred field $Y := G - \mu$ is a stationary Gaussian field.

When Cov satisfies the conditions of Theorem 2.1, we say that Cov is a valid covariance. In what follows we consider only the stationary GRF (or trend-stationary GRF), thus the stationary covariance function is noted to depend only on one variable $C(x)$. The Bochner's theorem provides the condition ensuring that C is a valid the stationary covariance.

Theorem 2.2. *(Bochner's theorem [3])*
A continuous function C defined in $\mathbb{R}^d$ is non-negative, if and only if there exists a decreasing, continuous, and bounded positive function S (spectral density) such that

$$C(x) = \int_{\mathbb{R}^d} e^{2i\pi p \cdot x} S(p) dp. \tag{1}$$

The formula (1) is the spectral representation of C which states that each valid covariance is the Fourier Transform of a positive function S called a spectral density. By isometry, this latter is given by the Fourier inverse of the covariance C,

$$S(p) = \int_{\mathbb{R}^d} e^{-2i\pi p \cdot x} C(x) dx. \tag{2}$$

Similar spectral representation of the GRF G states that there is a spectral complex Gaussian measure Z such that:

$$G(x, \cdot) = \int_{\mathbb{R}^d} e^{2i\pi px} Z(dp, \cdot), \tag{3}$$

where the measure Z has a zero mean and the variance $\mathbb{E}|Z(dp)|^2 = S(p)dp$.

2.1 Mean Square Continuity and Differentiability

We now describe the mean square continuity and differentiability of the random field G, following [1].

Definition 2.3. *A random field G is said to be mean square continuous if, for all $x \in D \subseteq \mathbb{R}^d$*

$$\lim_{h \to 0} \mathbb{E}[|G(x + h, \cdot) - G(x, \cdot)|^2] = 0,$$

It is said to be mean square differentiable if there is $Y := \dfrac{dG}{dx}$ such that:

$$\lim_{h \to 0} \mathbb{E}\left[\left|\frac{G(x + h, \cdot) - G(x, \cdot)}{h} - Y\right|^2\right] = 0,$$

In what follows, we consider the case when G is a stationary GRF with zero mean and unit variance. The regularity of such random field G is characterized by the regularity of the correlation function C [1, 23].

Proposition 2.1. *Let G be a stationary GRF with mean zero and unit variance.*

If C is continuous on $x = 0$, then G is mean-square continuous on D.

If C is differentiable on $x = 0$, then G is mean-square differentiable on D, and its derivative $\dfrac{dG}{dx}$ admits $-\dfrac{d^2C}{dx^2}$ as a correlation function.

By analogy, higher-order mean square derivatives of the field G can be defined, so when the $2m$th derivative of C exists around $x = 0$ then G is mth mean square differentiable. Note that mean square continuity or mean square differentiability does not necessarily yield to the continuity or the differentiability of sample paths of G, for a discussion of sample function continuity and differentiability see [1]. The smoothness of G can be characterized by the behaviour and the decay of the spectral density $S(p)$ as $|p| \to \infty$.

Proposition 2.2. *Let G be a stationary Gaussian random field defined by spectral density S. Suppose that S decrease at infinity with the bound:*

$$S(p) \leq \frac{K}{|p|^{m+1}} \tag{4}$$

for some $m > 0$. Then G is r-times mean square differentiable for each $r < \dfrac{m}{2} + \dfrac{1}{4}$.

Proof: A random field is r-times mean square differentiable if the covariance C is $2r$ times mean square differentiable.

The covariance function is given by the Fourier inverse of S, and if S satisfies the bound (4) then the function $p \to |p|^{2r} S(p)$ is square integrable on $\mathbb{R}^d$ if $r < \dfrac{m}{2} + \dfrac{1}{4}$, thus C is $2r$-times differentiable such that

$$\frac{d^{2r}C}{dx} = (2i\pi)^{2r} \int_{\mathbb{R}^d} p^{2r} S(p) e^{2i\pi px} dp.$$

■

3 Continuous Spectral Simulations

The spectral method uses the spectral representation given in the formula (3) to generate realizations of the GRF G. The method discretizes the integral (3) through the trapezium rule, in which a sequence of discrete spectral measure with amplitude S in the frequency domain are generated. Then, the Fourier inverse is performed to construct an approximation g_N of G on N equidistant points in D and constructed by superposition of N harmonic functions with random amplitude [17, 18, 19]:

$$g_N(x, \omega) := \sqrt{\Delta p} \sum_{k=1}^{N} \sqrt{S(p_k)} \Big(X_k(\omega) \cos(p_k x) + Y_k(\omega) \sin(p_k x) \Big), \tag{5}$$

where $(p_k)_{k=0}^N$ is an equidistant set of the frequencies points, Δp is the discretization step of the frequency domain, for $k = 1, \ldots, N$, X_k and Y_k are a sequence of independent Gaussian variables with zeros mean and unit variance. The discretization of the spectral density defined by the integral (1) suggests an approximation of G by the superposition of harmonic with random phase and deterministic amplitude as in [15, 18]:

$$\tilde{g}_N(x, \omega) = \sqrt{2\Delta p} \sum_{k=1}^{N} \sqrt{S(p_k)} \cos(p_k x + \varphi_k(\omega)). \tag{6}$$

Where $(\varphi_k)_{k=1}^N$ are independent random variables and uniformly distributed in $(0, 2\pi)$ Both those models have the same covariance and the ergodicity of the field is reached when $N \to \infty$. However, $\tilde{g}_N$ is asymptotically Gaussian for large N while g_N has a Gaussian distribution. Their covariance is only an approximation of the target continuous covariance C. It is shown in [19] that the simulated covariance converges with order $O(\frac{1}{N})$ to the target covariance for exponential model and with order $O(\frac{1}{N^2})$ for the Gaussian covariance model.

In what follows, we use the complex version of the approximation (5) which has a Gaussian distribution. The simulation is performed by the Discrete Fourier Transform and the analysis is more practice with the complex expansion. We discuss the convergence of the model regarding the length of the domain and the spatial discretization N, the regularity and the decay of its spectral density. Let $S(p)$ be the spectral density of G, let $\{x_0, \ldots, x_N\}$ be equidistant positions in $[0, L]$. Assuming that L and N is quiet large such that $P = \frac{N}{L}$ satisfies $S(p) \approx 0$ and $C(L) \approx 0$ where C is the covariance of G given by (1) and approximated by:

$$C(x) \approx \int_{-P}^{P} e^{2i\pi p \cdot x} S(p) dp. \tag{7}$$

We define the function $\tilde{S}$ on the box $[0, 2P]$ by:

$$\tilde{S} := \begin{cases} S(p) & \text{for } p \in [0, P/2], \\ S(P - p) & \text{for } p \in]P/2, P[. \end{cases}$$

We consider $p_0 = 0 < p_1 = \Delta < \ldots < p_{2N} = P$, a uniform discretization of the frequencies in $[0, P/2]$ and $\Delta p = \frac{1}{2L}$. Assuming that the position x is chosen such that $2Px$ is an integer, then equation (7) is equivalent to:

$$C(x) \approx \int_{0}^{P} e^{2i\pi p \cdot x} \tilde{S}(p) dp. \tag{8}$$

Therefore, by performing the trapezium approximation to the integral (8), the covariance function C is approximated by the following approximation:

$$C_N(x) \quad := \quad \Delta p \sum_{k=0}^{2N-1} \tilde{S}(p_k) e^{2i\pi p_k x} \tag{9}$$

Or equivalently with the co-sinus expansion we get,

$$C_N(x) \quad = \quad \Delta p (S(p_0) + S(p_N) \cos(2\pi p_N x)) + \frac{1}{L} \sum_{k=1}^{N-1} S(p_k) \cos(2\pi p_k x) \tag{10}$$

Now, we consider $\{\xi_k\}_{k=0}^{2N-1}$ to be a set of independent and complex Gaussian variables, where the real and imaginary part of each ξ_k have zero mean and unit variance and define the discrete Gaussian field G_N:

$$G_N(x,\cdot) := \sqrt{\Delta p}\sum_{k=0}^{2N-1}\sqrt{\tilde{S}(p_k)}e^{2i\pi p_k x}\xi_k. \tag{11}$$

Thus, the real and imaginary parts of G_N give an approximation of G as shown by the following proposition.

Proposition 3.1. *Both the real and imaginary part of G_N defined in (11) are independent Gaussian fields with zero mean, and admit C_N as a covariance function.*

Indeed, let G_N^* be the conjugate of G_N, $x1$ and x_2 in $[0,L]$, we have:

$$\begin{aligned}
\mathbb{E}[G_N(x_1)G_N(x_2)^*] &= \Delta p\mathbb{E}\Big[\Big(\sum_{k=0}^{2N-1}\sqrt{\tilde{S}(p_k)}e^{2i\pi p_k x_1}\xi_k\Big)\Big(\sum_{k=0}^{2N-1}\sqrt{\tilde{S}(p_l)}e^{-2i\pi p_l x_2}\xi_l^*\Big)\Big]\\
&= \Delta p\sum_{k,l=0}^{2N-1}\sqrt{\tilde{S}(p_k)\tilde{S}(p_l)}e^{2i\pi p_k(x_1-x_2)}\mathbb{E}[\xi_k\xi_l^*]\\
&= 2\Delta p\sum_{k=0}^{2N-1}\tilde{S}(p_k)e^{2i\pi p_k(x_1-x_2)} = 2C_N(x_1-x_2).
\end{aligned}$$

Since the real part and the imaginary part of ξ_k are independent, the real and imaginary part of $G_N(x)$ are independent and follow a Gaussian distribution with zeros mean and admit C_N as a covariance function. ■

The spectral approximation given by the expansion (11) can be seen as the complex version of the truncated Karhunen-Loève expansion [12] of a Gaussian field G_∞ defined by some covariance function Ψ. Indeed, this covariance is the periodization of C on the interval $[-L,L]$,

$$\Psi = \sum_{k\in\mathbb{Z}} C(x+2kL), \quad x\in[-L,L]$$

The set $\{\frac{1}{2L}e^{2i\pi p_k x}\}_{k=-\infty}^{\infty}$ form a complete system of the space $L^2([-L,L])$ and they are orthonormal eigenfunctions with their corresponding eigenvalues $\{S(p_k)\}_{k=-\infty}^{\infty}$ of the operator T_Ψ defined by,

$$T_\Psi(u(y)) := \int_{-L}^{L}\Psi(x-y)u(x)dx, \quad \forall u\in L^2([-L,L]),$$

Since we have,

$$\begin{aligned}
T_\Psi(e^{2i\pi p_k x}) &:= \int_{-L}^{L}\sum_{k\in\mathbb{Z}} C(x-y+2kL)e^{2i\pi p_k x}dx\\
&= e^{2i\pi p_k y}\int_{-\infty}^{\infty}C(x)e^{2i\pi p_k x}dx\\
&= S(p_k)e^{2i\pi p_k y}.
\end{aligned}$$

Therefore, The accuracy of the representation (11) depends on the finite spatial range L truncation of C and the truncated term $\frac{N}{L}$.

Remark 3.1. *The discretization (11) is very versatile when we sample numerous realizations of G with Monte-Carlo sampling since it gives two independent sample paths of G in each simulation. However, if we want to perform a deterministic sampling method such that Quasi-Monte Carlo methods [9] or sparse grid collocation method [8], it is crucial to use a real discretization of G from (5). This latter simulation is obtained from (4) by choosing the set $\{\xi_k\}_{k=0}^{2N-1}$ as real of independent standard variables and set $g_N = real(G_N) + Im(G_N)$ as a sum of real and imaginary part of G_N.*

The Continuous spectral method is performed using FFT algorithm only once time with easy implementation which is computed in $O(N\log(N))$ flops. First, we recall the DFT of any vector X with length N,

$$Y_n := \mathcal{F}(X)(n) = \sum_{k=0}^{N-1} X_k e^{\frac{-2i\pi kn}{N}},$$

and its inverse:

$$X_k = \mathcal{F}^{-1}(Y)(k) = \frac{1}{N}\sum_{n=0}^{N-1} Y_n e^{\frac{2i\pi kn}{N}}.$$

The $1d$-frequencies $\{p_k\}_{k=0}^{N}$ are given by $p_k = k\Delta p$ where $\Delta p = \frac{1}{2L}$. They are linked with the set of $N+1$ equidistant positions $\mathcal{H} := \{x_n\}_{n=0}^{N}$. The algorithm of the method is given as follows:

<u>*Unidimensional case*</u>

- Step 1. Sample the density S at the frequencies $\{p_k\}_{k=0}^{N}$.
- Step 2. Generate a Gaussian complex vector $\boldsymbol{\xi} = \xi_1 + i\xi_2$ of dimension $2N$, where the components of ξ_1 and ξ_2 have zero mean and unit variance.
- Step 3. Compute X the complex vector defined by $X_k = \boldsymbol{\xi}_k\sqrt{\Delta pS(p_k)}$, for $k = 0,\ldots,N$ and $X_k = \boldsymbol{\xi}_k\sqrt{\Delta pS(p_{2N-k})}$, for $k = N+1,\ldots,2N-1$.
- Step 4. Perform the iFFT of the vector $2NX$ to obtain a complex vector G_N. The real and imaginary parts of the first $N+1$ entries in G_N provide two independent realizations of the field G over the grid $\mathcal{H}$.

Not that by the symmetry of S and the set of the Gaussian variables, we can perform the FFT of the vector X.

<u>*Multi-dimensional case*</u>

The extension to $2d$ and $3d$ (or higher dimension) can be easily performed from one-dimensional simulations with tensor product. In the $2d$ simulation, consider $D = [0, L_1] \times [0, L_2]$ and consider the points $\{x_{k,l}\}_{l,k=1}^{N_1,N_2} \subset D$, and $\{p_{k,l}\}_{k,l=0}^{N_1,N_2}$ its

corresponding frequencies points defined by $p_{k,l} = (k\Delta p_1, l\Delta p_2)$, where $\Delta p_1 = \frac{1}{2L_1}$ and $\Delta p_2 = \frac{1}{2L_2}$ are the step-size in x-direction and y-direction respectively. Then the steps of the method are given by:

- Step 1. Sample the density S at $\{p_{k,l}\}_{k,l=0}^{N_1,N_2}$.
- Step 2. Generate a Gaussian complex matrix $\boldsymbol{\xi} = \xi_1 + i\xi_2$ of size $2N_1 \times 2N_2$, where the components of ξ_1 and ξ_2 have zero mean and unit variance.
- Step 3. Compute X the complex random matrix with $2N_1 \times 2N_2$ components, $X_{k,l} = \boldsymbol{\xi}_{k,l}\sqrt{\Delta p_1 \Delta p_2 S(p_{k,l})}$, $k = 0, \ldots, N_1$, $l = 0, \ldots, N_2$ and $X_{k,l} = \boldsymbol{\xi}_{k,l}\sqrt{\Delta p_1 \Delta p_2 S(p_{2N_1-k,2N_2-l})}$, $k = N_1+1, \ldots, 2N_1-1$, $l = N_2+1, \ldots, 2N_2-1$.
- Step 4. Perform the $2d$ FFT of the matrix X to obtain a complex matrix G_N. The real and imaginary parts of the first $(N_1 + 1) \times (N_2 + 1)$ entries in G_N give two independent realizations of G over the grid $\mathcal{H}$.

The method uses FFT algorithm, which provide a discrete field G_N at equidistant points only with $O(N \log(N)$ operations. Thus, simulations with this method is greatly fast, and in some case it can be very efficient regardless methods using a matrix factorization. Sampling of the field on non-uniformly spaced sample positions $\mathcal{K}$ can obtained by simulating G with spectral simulation on a given smallest grid which cover the set positions $\mathcal{K}$ and then extract the desired positions form G_N. In section which follows we discuss the errors bounds (weak and strong error estimate) of the method regarding the smoothness of the field G and its spectral density S.

4 Error estimation and convergence

4.1 Decay rate of the covariance function

The spectral method is very fast regardless methods based on the decomposition of the covariance matrix. However, the method is not exact, which means that the covariance matrix of the discrete G_N is only an approximation of the target covariance C. In this section, we show that both convergence (strong and weak) is very fast regardless of the decay of S and C to zero. Given the convergence of Fourier series [4], the continuous spectral representation method convergence either with geometric or algebraic decay. For a sake of clarity of the presentation, we provide the error estimate of the spectral method in $1d$-dimensional simulation, the case of $2d$ and $3d$ the convergence is concluded as sum of the error interpolation in each direction. First, we characterize the decay of the covariance C at infinity, it is linked with the regularity of the spectral density S.

For each positive real $s > 0$, we define the following Sobolev space:

$$H^s(\mathbb{R}) := \left\{u \in L^2(\mathbb{R}); (1 + |x|^s)\hat{u} \in L^2(\mathbb{R})\right\},$$

where $\hat{u}$ denotes the Fourier transform of the function u. The regularity of the spectral density S provides the way in which the covariance function C behaves at

infinity. The following Lemma characterizes this decay of C regarding the smoothness of S.

Lemma 4.1. *Suppose that S belongs in $H^s(\mathbb{R})$ for some $s > 0$. Then, there exists $K_1 > 0$ such that C decreases at infinity with the following decay bound,*

$$C(x) \leq \frac{K_1}{|x|^{s+\frac{1}{2}}}, \qquad x > 0. \tag{12}$$

Proof: Since S belongs in $H^s(\mathbb{R})$ and C its Fourier transform, Thus, the function $(1 + |x|^s)C$ is square integrable, then at least it decreases at infinity with the decay bound $(1 + |x|^s)C \sim \frac{1}{|x|^\epsilon}$ for some $\epsilon > \frac{1}{2}$, thus there exists $K_1 > 0$ which depends only on s such that $|C(x)| \leq \frac{K_1}{|x|^{s+\frac{1}{2}}}$. ■

The decay rate to zero at infinity of the covariance C is better when the sth derivative of S has a bounded variation as states the following Lemma.

Lemma 4.2. *Suppose that S has s continuous derivatives in the space $L^2(D)$ such that the derivative $\frac{d^s S}{dp^s}$ has a bounded variation. Then, there exists $K_2 > 0$ such that C decreases at infinity with the decay bound:*

$$C(x) \leq \frac{K_2}{|x|^{s+1}}, \qquad x > 0. \tag{13}$$

Proof: The sth derivative of the spectral density S has a bounded variation, so its Fourier transform $\widehat{\frac{d^s S}{dp^s}}$ decreases at infinity with the bound $O(\frac{1}{x})$ (see [**?**]) and satisfies $\widehat{\frac{d^s}{dp^s}S} = (2i\pi x)^s C$. Therefore, there exists $K_2 > 0$ which depends on s such that $|C(x)| \leq \frac{K_2}{|x|^{s+1}}$. ■

When the spectral density is infinitely differentiable i.e. $s = \infty$, the covariance function C decreases fast and exponentially at infinity like the following decay bound,

$$C(x) \leq K_3 e^{-qx^r}, \qquad x > 0. \tag{14}$$

for some non-negative real numbers $q > 0$, $r > 0$ and $K_3 > 0$.

Similarly, we can predict the decay rate of the spectral density S at infinity from the smoothness of the covariance function C. The density S has an algebraic decay when C belongs in $H^m(\mathbb{R})$ and an exponential decay when C is infinitely differentiable.

4.2 Weak error estimate

The covariance of the discrete GRF G_N from (11) admits the function C_N in (9) as a covariance which is seen as the classical trapezium approximation of the integral (8). In [13] it is shown that C_N converges to C with a bound $O(\frac{1}{L})$ or with the bound $O(\frac{1}{L^2})$ under some additional assumption on the smoothness of S and the decay of its derivatives. Both these bounds are given up a neglected truncated range error $O(\frac{L}{N^m})$. On the other hand, the error of the spectral method is expected

in [18, 19] to decay with the bound $O(\frac{1}{N^2})$. Further, all the constant of these error bounds increase with the length of the spatial domain.

The theorem 4.2 provides an optimal bound of the method. The field G_N can be seen as a truncated Karhunen-Loève decomposition of a Gaussian field with a covariance function Ψ, the periodization of C on a spatial box $[-L, L]$ for some L in which the discrete covariance is valid. Therefore, the error is decomposed on two contributions, the discretized error and the truncated error, the first one depends on the smoothness of the GRF G (described by the decay of S) and the second one depend on the smoothness of S.

We assume that the correlation length $\theta = 1$ (without loss of generality, by changing the size L by L/θ). The following Theorem gives an algebraic decay of the error bound on the covariance of the spectral simulation in the box $(-L, L)$,

Theorem 4.1. *Suppose that S belongs in $H^s(\mathbb{R})$ and satisfies the decay condition (4). Then the discrete covariance function C_N defined in (9) converges to C as:*

$$\|C - C_N\|_{L^\infty([-L,L])} \leq \kappa \left[\left(\frac{L}{N} \right)^m + \frac{1}{L^{s+1}} \right]. \tag{15}$$

Where the constant κ depends only on m and s (independent of L and N).

Proof:

Consider the periodization of the covariance C on $\mathbb{R}$ defined (a.e) in $(-L, L)$:

$$\Psi(x) := \sum_{k=-\infty}^{\infty} C(x + 2kL),$$

since $\Psi(x + 2L) = \Psi(x)$, the function Ψ is $2L$-periodic. Therefore, its Fourier series representation is given by:

$$\Psi(x) = \sum_{k=-\infty}^{\infty} \psi_k e^{2i\pi p_k x},$$

where each Fourier coefficient ψ_k satisfies:

$$\begin{aligned} \psi_k &:= \frac{1}{2L} \int_{-L}^{L} \Psi(x) e^{-2i\pi p_k x} dx \\ &= \frac{1}{2L} \int_{\mathbb{R}} C(x) e^{-2i\pi p_k x} dx \\ &= \Delta p S(p_k). \end{aligned}$$

Since the function S is even, the expansion of Ψ is reduced on the cousins basis,

$$\Psi = \frac{1}{2L} S(p_0) + \frac{1}{L} \sum_{k=1}^{\infty} S(p_k) \cos(2\pi p_k x).$$

Now, considering its truncated function

$$\Psi_N := \frac{1}{2L} (S(p_0) + S(p_N) \cos(2\pi p_N x)) + \frac{1}{L} \sum_{k=1}^{N-1} S(p_k) \cos(2\pi p_k x) = C_N.$$

Then, the following estimate hold:

$$\|\Psi - C_N\|_\infty \leq \frac{1}{L} \sum_{k=N}^{\infty} S(p_k).$$

By using the bound from (4), we get a bound of the error due to the frequencies truncation,

$$\|\Psi - C_N\|_\infty \leq \frac{K 2^{m+1}}{m} \left(\frac{L}{N}\right)^m. \tag{16}$$

The error due to the finite spatial range is quantified by $\|C(x) - \Psi(x)\|_{L^\infty([-L,L])}$, thus for each $x \in [-L, L]$,

$$|C(x) - \Psi(x)| = \left| \sum_{k=1}^{\infty} C(x + 2kL) + \sum_{k=-\infty}^{-1} C(x + 2kL) \right|$$

From the bound (13), we obtain:

$$\begin{aligned} |C(x) - \Psi(x)| &\leq \sum_{k=1}^{\infty} |C(x + 2kL)| + \sum_{k=-\infty}^{-1} |C(x + 2kL)| \\ &\leq \frac{1}{L^{s+1}} \sum_{k=1}^{\infty} \frac{2K_2}{(2k-1)^{s+1}} \\ &\leq \frac{K_2}{sL^{s+1}} \end{aligned} \tag{17}$$

On the other hand we have,

$$\|C - C_N\|_{L^\infty([-L,L])} \leq \|C - \Psi\|_{L^\infty([-L,L])} + \|\Psi - C_N\|_{L^\infty([-L,L])}$$

Therefore, the estimate of Theorem 4.1 follows by combining the upper bounds (16) and (17). ■

From the estimate of Theorem4.1, the convergence of C_N to C is given by the decay of the spectral density S and the covariance C to zero. It depends on $1/L$ (error due to the space truncation) and the ratio $\frac{L}{N}$ (error due to the frequency truncation). The size N is controlled by the decay of S at infinity and L is controlled by the decay of C. Therefore, when C and S decrease rapidly to zeros at infinity, the Spectral method becomes effective and more attractive.

When the random field has infinite derivatives in the quadratic sense, the spectral density S decays exponentially to zeros at infinity. Further, the covariance function C decays exponentially if the density S is infinitely differentiable. In such case the continuous spectral method is very efficient since it provides accurate simulations even with small length L and a small number N of points of discretization.

The following proposition gives the estimate error of the method in the week sense when both G and S are infinitely differentiable.

Proposition 4.1. *Suppose that both S and C decay exponentially to zero at infinity with the following bounds*

$$S(p) = O(e^{-2q_s p^r}), \quad C(x) = (Oe^{-q_c x^\nu}), \qquad q_s, q_c > 0, r, \nu > 0 \tag{18}$$

Then the discrete covariance function C_N defined in (9) converges geometrically to C with the bound:

$$\|C - C_N\|_{L^\infty([-L,L])} \leq \hat{\kappa}\left(e^{-q_s(\frac{N}{L})^r} + e^{-q_c L^\nu}\right). \tag{19}$$

The constant $\hat{\kappa}$ is independent of L and N.

The proof of the estimate 19 is similar to the proof of the Theorem 4.1 by using adequately the exponential decays (18).

4.3 Error in the norm of $L^2(\Omega)$

The continuous spectral method converges in L^2 norm (strong convergence) when the ratio $N/L \to \infty$ together with $L \to \infty$. The strong error is defined by the root-mean-square quantity $\|G - G_N\|_{L^2(\Omega,\mathbb{C})} := (\mathbb{E}[|G - G_N|^2])^{\frac{1}{2}}$. The following theorem provides the upper bound of the error in the $L^2(\Omega)$-norm. It is similar to the upper bound in (15) up the power $1/2$.

Theorem 4.2. *Suppose that S belongs in $H^s(\mathbb{R})$ and satisfies the decay condition (4). Further assume that C is convex on $[L, \infty]$. Then the discrete GRF G_N from (11) converges to G with the following bound:*

$$\|G - G_N\|_{L^2(\Omega,\mathbb{C})} \leq \tilde{\kappa}\left[\left(\frac{L}{N}\right)^{\frac{m}{2}} + \left(\frac{1}{L}\right)^{\frac{s+1}{2}}\right]. \tag{20}$$

The constant $\tilde{\kappa}$ depends only on m and s (independent of L and N).

Proof:

In order to compare G with G_N within $\mathcal{E} := \|G - G_N\|_{L^2(\Omega,\mathbb{C})}$ the mean-squared error, we develop G on the Discrete Fourier basis. For this reason G is expanded by the circulant embedding approach which is an exact representation under the sufficient condition of non-negative definite. Therefore, following representation of G holds through the circulant embedding approach [5, 7, 13] :

$$G(x_n) = \sum_{k=0}^{2N-1} \frac{1}{\sqrt{2N}} \sqrt{d_k} e^{2i\pi p_k x_n} \xi_k, \qquad n = 0, 1, \ldots, N,$$

here, each coefficient d_k equals,

$$d_k = \sum_{n=0}^{2N-1} \tilde{C}_n e^{-2i\pi p_k x_n}$$

were we define the vector $\tilde{C} := (C(x_0)\ldots, C(x_N), C(x_{N-1}), \ldots, C(x_1)))$. Therefore, the square of the error $\mathcal{E}^2$ is bounded by,

$$\begin{aligned}\mathcal{E}^2 &= \sum_{k=0}^{2N-1}\left(\frac{1}{\sqrt{2N}}\sqrt{d_k} - \sqrt{\triangle p}\sqrt{S(p_k)}\right)^2 \qquad (21)\\ &\leq \triangle p \sum_{k=0}^{2N-1}\left|\frac{1}{P}d_k - \tilde{S}(p_k)\right| \\ &\leq \frac{1}{L}\sum_{k=0}^{N}\left|\frac{1}{P}d_k - S(p_k)\right| \qquad (22)\end{aligned}$$

where $P = \frac{N}{L}$, $p_k = k\triangle p$, $x_n = \frac{n}{P}$. Now, considering the periodization of the spectral density S which is P-periodic and defined (a.e) in the interval $(-\frac{P}{2}, \frac{P}{2})$:

$$\mathfrak{S}(p) := \sum_{l=-\infty}^{\infty} S(p + lP),$$

its Fourier series representation at each p_k is given by:

$$\begin{aligned}\mathfrak{S}(p_k) &= \sum_{n=-\infty}^{\infty} s_n e^{-2i\pi p_k x_n} \\ &= \frac{d_k}{P} + C(x_N)\cos(2\pi p_k x_N) + \frac{2}{P}\sum_{n=N+1}^{\infty} C(x_n)\cos(2\pi p_k x_n)\end{aligned}$$

since each Fourier coefficient s_n satisfies the equation

$$\begin{aligned}s_n &:= \frac{1}{P}\int_{-P/2}^{P/2}\mathcal{S}(p)e^{2i\pi p x_n}dp \\ &= \frac{1}{P}\int_{\mathbb{R}} S(p)e^{2i\pi p x_n}dx = \frac{1}{P}C(x_n).\end{aligned}$$

Therefore, by substituting the term $\frac{d_k}{P}$ in the bound (22) the error $\mathcal{E}^2$ is decomposed in two parts as follows,

$$\mathcal{E} \leq \frac{1}{N}\sum_{k=0}^{N}\underbrace{\left|C(x_N)\cos(2p_k x_N) + 2\sum_{n=N+1}^{\infty} C(x_n)\cos(2p_k x_n)\right|}_{I_k} + \underbrace{\frac{1}{L}\sum_{k=0}^{2N}\left|S(p_k) - \mathfrak{S}(p_k)\right|}_{II}\Bigg) \qquad (23)$$

The second term II of the error $\mathcal{E}^2$ is due to the discretization, it can be bounded

by using the decay rate of the spectral density as follows,

$$\begin{aligned} II &\leq \frac{1}{L}\sum_{k=0}^{N}\sum_{l\in\mathbb{Z}^*} S(p_k + lP) \\ &\leq \frac{2}{L}\sum_{k=0}^{N}\sum_{l=1}^{\infty} \frac{1}{(-p_N + lP)^{m+1}} \\ &\leq \frac{2}{L}\sum_{k=0}^{N}\left(\frac{L}{N}\right)^{m+1}\sum_{l=1}^{\infty}\frac{1}{(l+0.5)^{m+1}} \\ &\leq \frac{2^{m+2}}{3^m m}\left(\frac{L}{N}\right)^m \end{aligned} \tag{24}$$

From the decay rate of the covariance function C in (13), the partial term of the error due to the range truncation I_k is finite and independent of N. In order to bound the total error of the range truncation $\sum_{k=0}^{N} I_k$, we first introduce the Dirichlet and Féjer kernels

$$D_n(\nu) := \begin{cases} \displaystyle\sum_{k=0}^{N}\alpha_k\cos(2\pi k\nu) = \frac{\sin(\pi\nu(2n+1))}{\sin(\pi\nu)} & \text{if } \nu \in \mathbb{R}/2\pi\mathbb{Z} \\ 2n+1 & \text{if } \nu \in 2\pi\mathbb{Z} \end{cases}$$

$$F_n(\nu) := \sum_{l=0}^{n} D_l(\nu) = \left(\frac{\sin(\pi\nu(n+1))}{\sin(\pi\nu)}\right)^2$$

We also define the error term $J_k := \displaystyle\sum_{n=0}^{\infty}\alpha_n C(L+x_n)\cos(2p_k x_n)$ where the coefficients $\alpha_0 = 1$, $\alpha_n = 2$ for $n > 0$ and eventually we have $|J_k| = I_k$. Upon Abel's summations by parts, each partial term J_k is positive, Indeed,

$$\begin{aligned} J_k &= \sum_{n=0}^{\infty}\Big(C(L+x_n) - C(L+x_{n+1}))\Big)D_n(k/2N) \\ &= \Big|\sum_{n=0}^{\infty}\Big(C(L+x_n) - 2C(L+x_{n+1}) + C(L+x_{n+2})\Big)F_n(k/2N) \geq 0 \end{aligned}$$

since C is convex for $x > L$, the term $C(L+x_n) - 2C(L+x_{n+1}) + C(L+x_{n+2})$ is positive and the Féjer kernels are non-negative. Therefore we get,

$$I_k = \sum_{n=0}^{\infty}\alpha_n C(L+x_n)\cos(2p_k x_n) \tag{25}$$

The total error of the range truncation satisfies the following equations,

$$\begin{aligned} \sum_{k=0}^{N} I_k &= \sum_{n=0}^{\infty} C(L+x_n)\sum_{k=0}^{N} a_k\cos(2\pi kn/2N) \\ &= \sum_{n=0}^{\infty} C(L+x_n)D_N(n/2N) \end{aligned}$$

since $D_N(n/2N) = 2N+1$ if n is a multiple of $2N$ and $D_N(n/2N) = (-1)^n$ otherwise, we get:

$$\sum_{k=0}^{N} I_k \;=\; \sum_{n=0}^{\infty}(-1)^n C(L+x_n) + 2N\sum_{l=0}^{\infty} C((2l+1)L)$$

by using the decay rate of C from (13), the total error of the range truncation is bounded by,

$$\begin{aligned}\frac{1}{N}\sum_{k=0}^{N} I_k &\leq \frac{1}{NL^{s+1}}\int_0^{\infty}\frac{1}{(1+x/N)^{s+1}}dx + \frac{2}{L^{s+1}}\int_0^{\infty}\frac{1}{(2x+1)^{s+1}}dx \\ &\leq \frac{2}{s}\frac{1}{L^{s+1}} \end{aligned} \tag{26}$$

Therefore, by combining estimates (24) and (26) we get,

$$\mathcal{E}^2 \leq \tilde{\kappa}^2\left[\left(\frac{L}{N}\right)^m + \frac{1}{L^{s+1}}\right], \tag{27}$$

where $\tilde{\kappa}^2 := \max(\frac{2}{s}, \frac{2^{m+2}}{3^m m})$. Thus the estimate of Theorem 4.2 follows by taking the square root of the bound 27. ■

From the estimate of Theorem4.2, the convergence of G_N to G in the $L^2(\Omega)$-norm is algebraic when the spectral density S and the field G are both smooth. Further, when they are both infinitely differentiable, the convergence of G_N to G in the $L^2(\Omega)$-norm is sub-geometric as provided by the following proposition.

Proposition 4.2. *Suppose that both S and C decay exponentially to zero at infinity with the bounds*

$$S(p) = O(e^{-2q_s p^r}), \quad C(x) = (Oe^{-2q_c x^\nu}), \qquad q_s, q_c > 0, r, \nu > 0 \tag{28}$$

Then the discrete covariance function C_N defined in (9) converges to C with bound:

$$\|G - G_N\|_{L^2(\Omega,\mathbb{C})} \leq \bar{\kappa}\left(e^{-q_s(\frac{N}{L})^\nu} + e^{-q_c L^r}\right). \tag{29}$$

The constant $\bar{\kappa} > 0$ is independent of L and N.

The proof of the estimate (29) is similar to the proof of the Theorem 4.2 by using adequately the exponential decays (28).

5 Numerical example

In this section we provide numerical experiments to illustrate the theoretical estimates of the continuous spectral method detailed above. We consider realizations of $1d$ and $2d$ Gaussian random field G with zero mean, unit variance and defined by the Matérn covariance model.

5.1 Matérn-Whittle model

The Matérn covariance functions are the commonly used model in the practice for the Gaussian field. There are got from the Matérn model of the following spectral densities:

$$S(p) = \frac{\alpha}{(\theta^2 + |p|^2)^{\nu+d/2}} \tag{30}$$

where the parameters ν, α and θ are non-negative real numbers, d is the space dimension, the parameter θ is the correlation length and p is a wave vector in $\mathbb{R}^d$.

The corresponding covariance (Matérn model) of this spectral density S is given by the following function:

$$C(r) = \frac{2^{\nu-1}}{\Gamma(\nu)} \left(\frac{\sqrt{2}\nu r}{\theta} \right)^{\nu} \mathcal{K}_\nu \left(\frac{\sqrt{2}\nu r}{\theta} \right) \tag{31}$$

where r is the Euclidean distance between two points, $\mathcal{K}_\nu$ denotes the modified Bessel function of the second kind and Γ is the gamma function. When $\nu = \frac{1}{2}$ the Matérn covariance coincides with the exponential covariance, $c(r) = e^{-r/\theta}$ which is a Hölder continuous function. When $\nu \longrightarrow \infty$, the Matérn covariance approaches the Gaussian covariance, $c(r) = e^{-r.^2/(2\theta^2)}$. In this case, the covariance is an analytic function as far as the sample paths of the Gaussian field are also analytic, almost everywhere in Ω.

The non-negative parameter $\nu > 0$ characterizes the smoothness of C, as far as the mean-square differentiability of the field G. Indeed, this can be seen from the decay rate of the spectral density S which is polynomial decay or exponential decay when ν approaches the infinity. Further, there is a roughness of G for a small value of ν, say $\nu \leq 1$. Furthermore since the spectral density function is infinitely differentiable, the Matérn model decreases exponentially with the length of the domain. Figure1 illustrates this decay for both functions with four values of the parameter ν.

5.2 Generation of 1D field

Here we consider for the clarity of the illustration, the correlation length $\theta = 1$ and the space domain is meshed with N equidistant points to perform the FFT algorithm. Figure 2 gives examples of realizations of $1d$ generated Gaussian fields defined by the spectral density S (30), with four values of the parameter ν. Each simulation is the real and imaginary part of the discrete field in (11). We remark the path is rough for both cases $\nu = \frac{1}{2}$ and $\nu = 1$, the sample path is smooth for $\nu = 4$ and $\nu = \infty$.

Both the upper bounds for weak and strong convergence decay to zero when the space length $L \to \infty$ and the frequency length $P = \frac{N}{L} \to \infty$. Further, all the constants in the upper bound for the error are independent of L and $P = \frac{N}{L}$ in

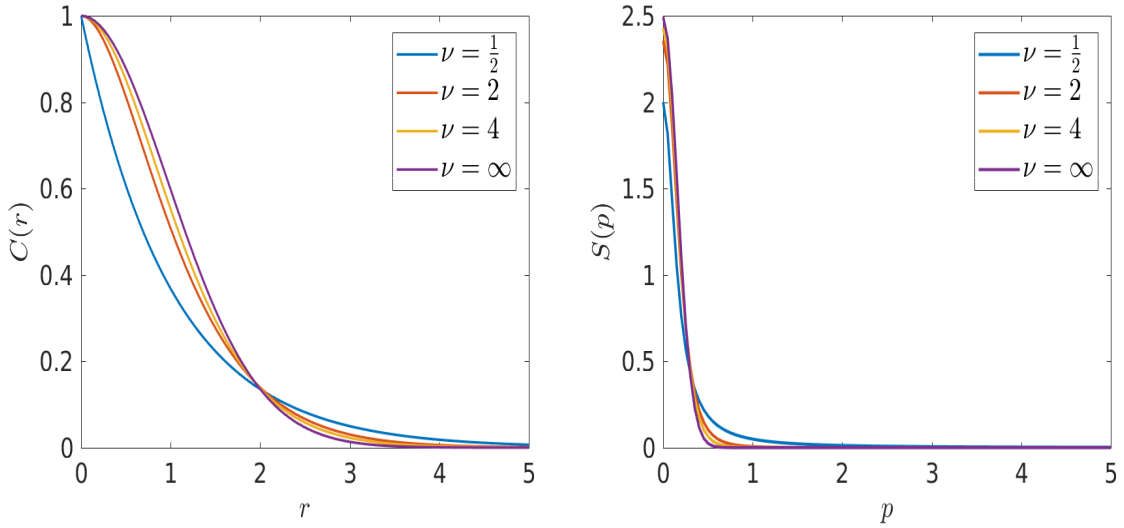

Figure 1: Matérn covariance function $C(r)$ (left), Spectral density $S(p)$ (right)

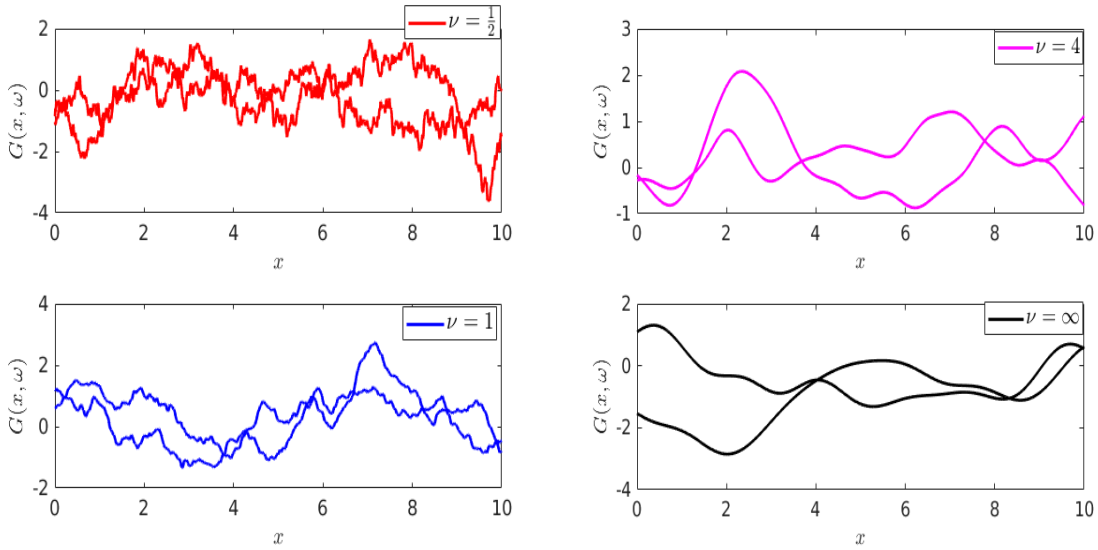

Figure 2: Examples of generated Gaussian fields with $N = 400$.

both theorems. In order to illustrate the behaviour of the the weak error of the continuous spectral method with respect to L and P; we consider the case when $\nu = \frac{1}{2}, 1, 4$, and $\nu = \infty$. First we analyse the error with respect to P by fixing the length $L = 20$ in which the space-truncated error is neglected since $C(x)$ decreases exponentially to zeros as $x \to \infty$. Figure3 illustrate The absolute error $|C - C_N|$ between the covariance C from (31) and the approximation C_N from (10), with $N = 400$, It shows that the error decreases when ν increases since the decay of the spectral density decreases with ν. Figure10 plots the covariance matrix of G_N

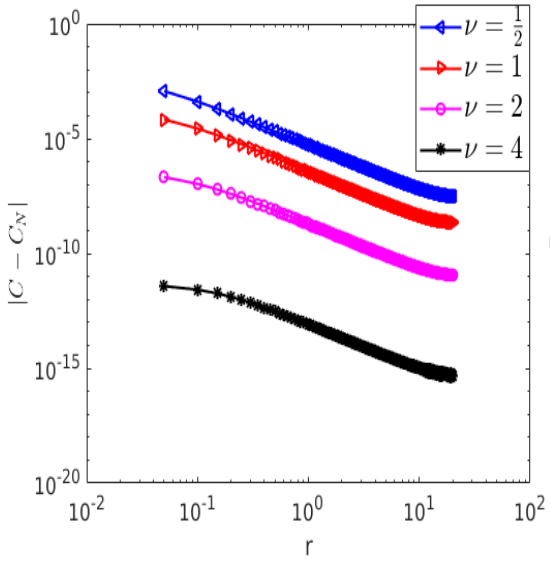

Figure 3: absolute error $|C - C_N|$, $N = 400$ and $L = 20$

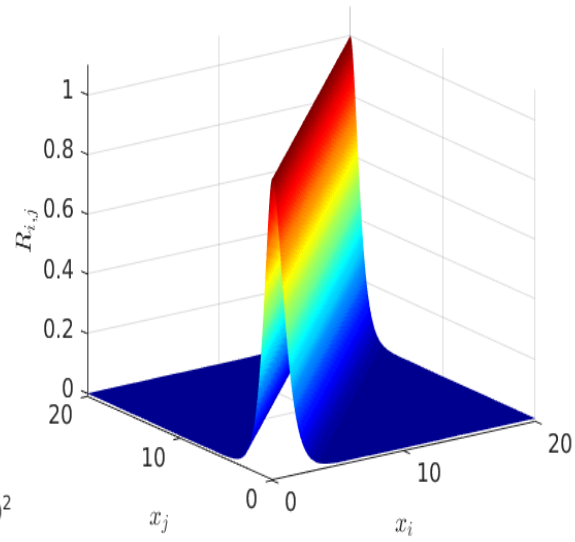

Figure 4: Covariance matrix with MC sampling, $\nu = 2, N = 400$ and $L = 20$.

computed with MC sampling from (33) through $M = 10^6$ MC simulations. Figure

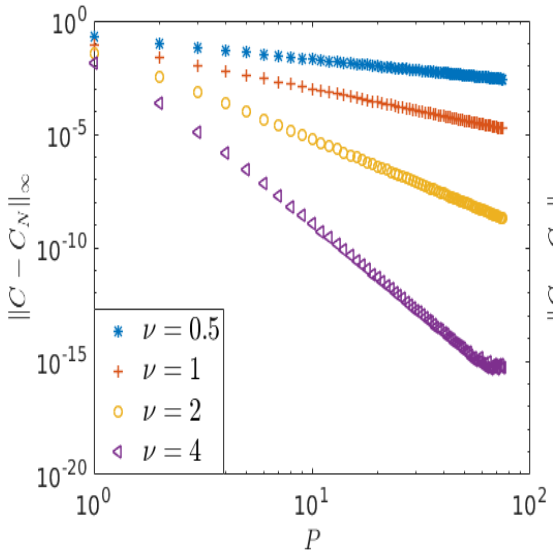

Figure 5: $\|C - C_N\|_\infty$ with respect to P.

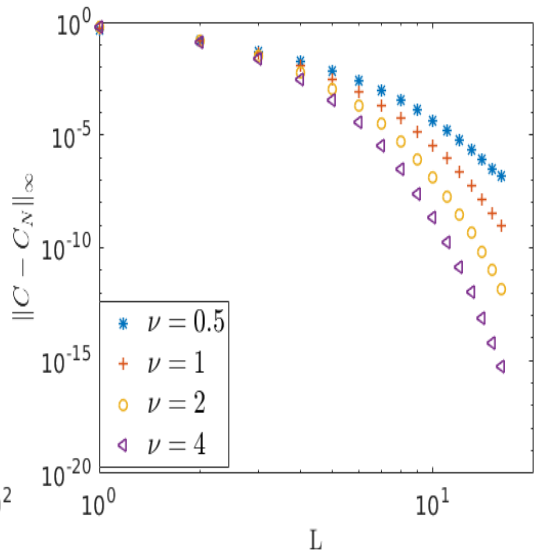

Figure 6: $\|C - C_N\|_\infty$ with respect to L.

5 plots the error $\|C - C_N\|_\infty := \max_{0 \le x \le L} |C(x) - C_N(x)|$ as function of the length of the frequencies domain $P = (1 : 1 : \frac{N}{L})$. As expected, figure shows that the error with respect to P is algebraic since the spectral density S decreases algebraically as

p becomes large. Figure14 plots the error $\|C - C_N\|_\infty$ with respect of the length of the space domain $L = (1 : 1 : 15)$.,In each case of ν we take a large number of equidistant points N to overcome the error due to the discretization (frequency domain truncation). As expected, figure shows that the error with respect to L is sup-geometric since the covariance function decreases exponentially at infinity.

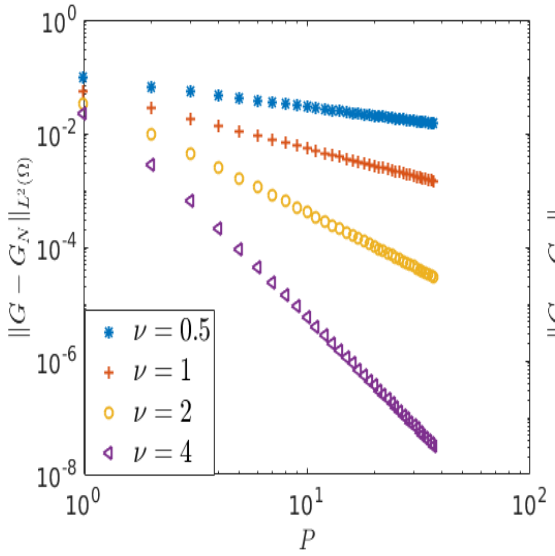

Figure 7: $\|G - C_N\|_{L^2(\Omega)}$ with respect to P.

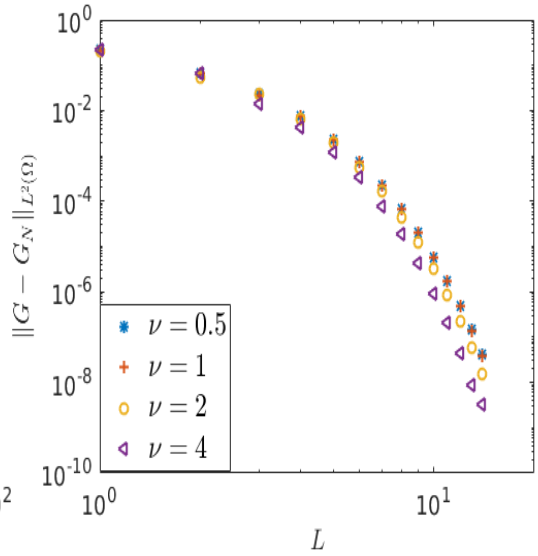

Figure 8: $\|G - C_N\|_{L^2(\Omega)}$ with respect to L.

Figure7 illustrates the theoretical bounds of the strong error $\|G - G_N\|_{L^2(\Omega)} := \sqrt{\mathbb{E}[|G - G_N|^2]}$, as computed in (22). This bound is illustrated with respect of the length of the frequency domain $P = (1 : 1 : \frac{N}{L})$. As expected, figure shows that the error with respect to P is algebraic. Figure8 plots the bound of the strong error $\|C - C_N\|_\infty := \max_{0 \geq x \leq L} |C(x) - C_N(x)|$ as function of L the length of the space domain $L = (1 : 1 : 15)$, where for each case of ν we take a large number of equidistant points N to overcome the error due to the discretization (frequency domain truncation). As expected, figure shows that the error with respect to L is sup-geometric. Further, theses figures shows that the strong error is large than the weak error (error on the covariance) as illustrated in Figures 5 and 14, this is because the power $\frac{1}{2}$ in the bound of strong error.

In order to illustrate the accuracy of the method from numerical simulations, we computed the error bound from sampling simulations of the field G_N. Therefore, the discrete covariance C_N from (9) by Monte-Carlo sampling. However, because the statistical error of the MC is very slow ($O(\frac{1}{\sqrt{M}})$, A large number of MC simulations is needed to reach a very small precision. For this raison, we consider the case where the field is not differentiable for example $\nu = \frac{1}{2}, 1, 2$. We recall that the discrete covariance function of the discrete field G_N is estimated by the MC sampling with

average sum:

$$C_N(x_i) \approx \frac{1}{M} \sum_{l=1}^{M} G_N(x_i, \omega_l) G_N^*(x_0, \omega_l) \tag{32}$$

and the covariance matrix by the following average,

$$R_N(i,j) \approx \frac{1}{M} \sum_{l=1}^{M} G_N(x_i, \omega_l) G_N^*(x_j, \omega_l) \tag{33}$$

Figure9 illustrates the error on the covariance $\|C - C_N\|_\infty$ of the continuous spectral method as function of the frequency step from $P = 1$ to $P = \frac{N}{L}$, where $N = 100$ and $L = 10$. The discrete covariance is computed from (32) by simulating $M = 10^{10}$ trajectories of G_N in order to hide the statistical error due to the MC sampling. Figure10 plots $\|C - C_N\|_\infty$ with respect to the space step from $L = 1$ to $L = 10$, where $N = 100$ for each step. Similarly, the discrete covariance is computed from (32) by simulating $M = 10^{10}$ trajectories of G_N. However as we can see from the figure the statistical error du to MC sampling is not removed with $M = 10^{10}$ for $L = 10$ since the error on the covariance decays exponentially with L. Both upper bounds for the approximation error converge to zero as L and P become large. We can conclude from the value of the error at the origin that all the constants in the upper bound are very small and independent of N and L. The predicted growth of the covariance error is clearly seen in Figure 9 and 10.

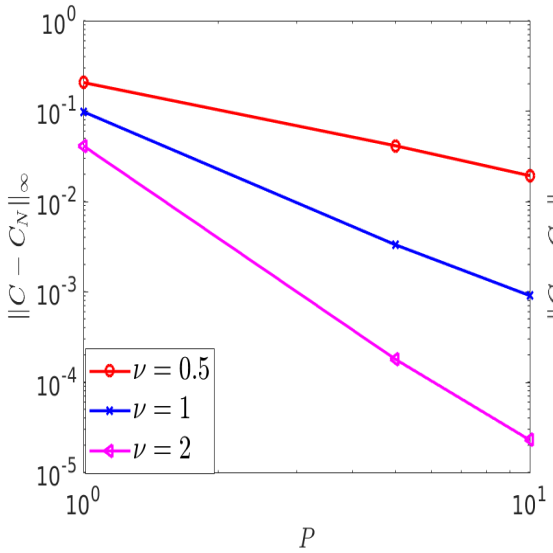

Figure 9: $\|C - C_N\|_\infty$ with respect to P.

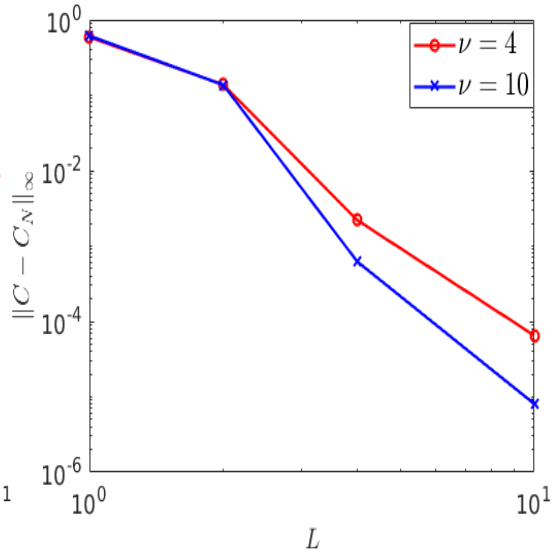

Figure 10: $\|C - C_N\|_\infty$ with respect to L.

5.3 Generation of 2D field

Here we consider a standard and isotropic Gaussian field G with correlation length $\theta = 1$ and defined by the covariance model from (31). The space domain is

the square $D := [0, L_x] \times [0, Ly]$ and meshed with $Nx \times Ny$ equidistant points to perform the FFT algorithm. Figure 11 gives examples of realizations of G as detailed in the algorithm of Section 3 , with two values of the parameter $\nu = \frac{1}{2}$ and $\nu = 4$. We remark a roughness of the path for $\nu = \frac{1}{2}$ and a smoothness of the sample path for $\nu = 4$.

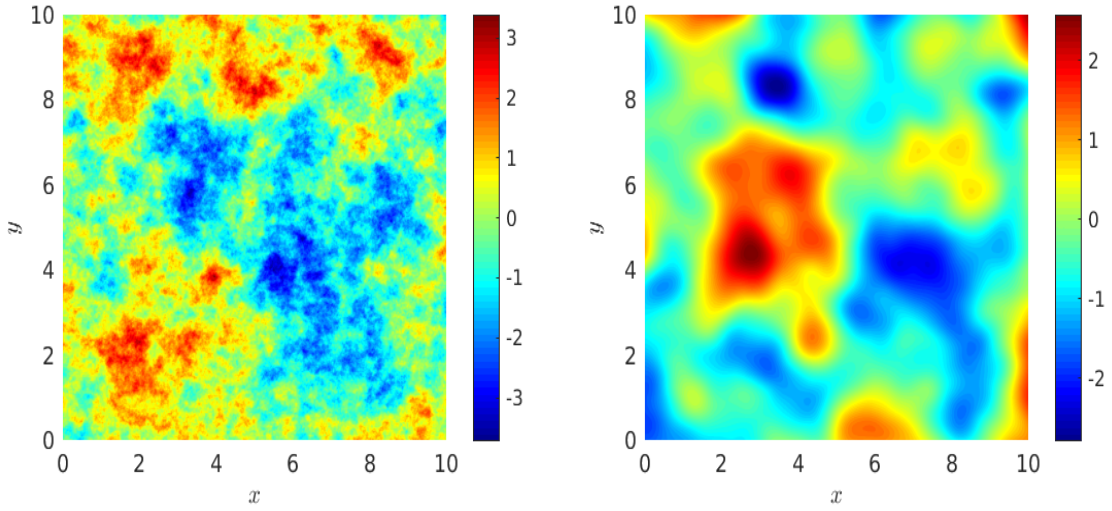

Figure 11: Two realization of Gaussian field with spectral method (left: $\nu = \frac{1}{2}$, right: $\nu = 4$) $L_x = 10, L_y = 10$ and $Nx = Ny = 200$.

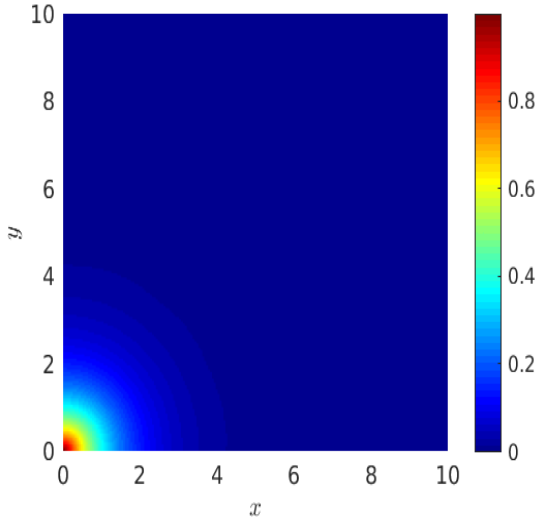

Figure 12: C_N with MC sampling.

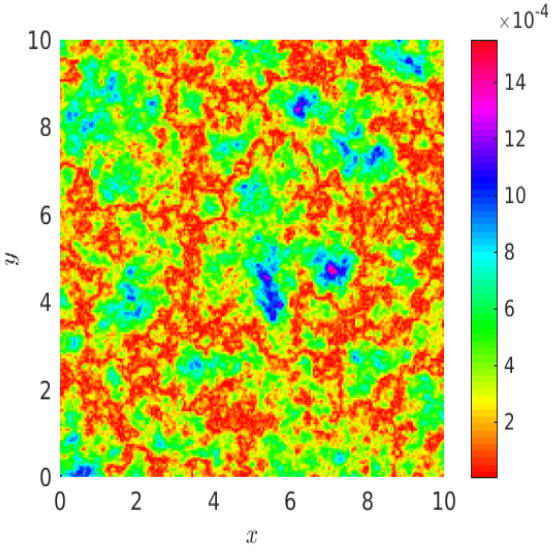

Figure 13: Absolute error $|C - C_N|$ with MC sampling

Figure13 illustrates the absolute error $|C - C_N|$ between the covariance C from (31) and the discrete covariance C_N computed using MC sampling from (33) which is plotted in Figure 12 with $\nu = \frac{1}{2}$, $Nx = Ny = 300$, and $L_x = L_y = 10$. The approximation is performed with $M = 10^6$ MC simulations.

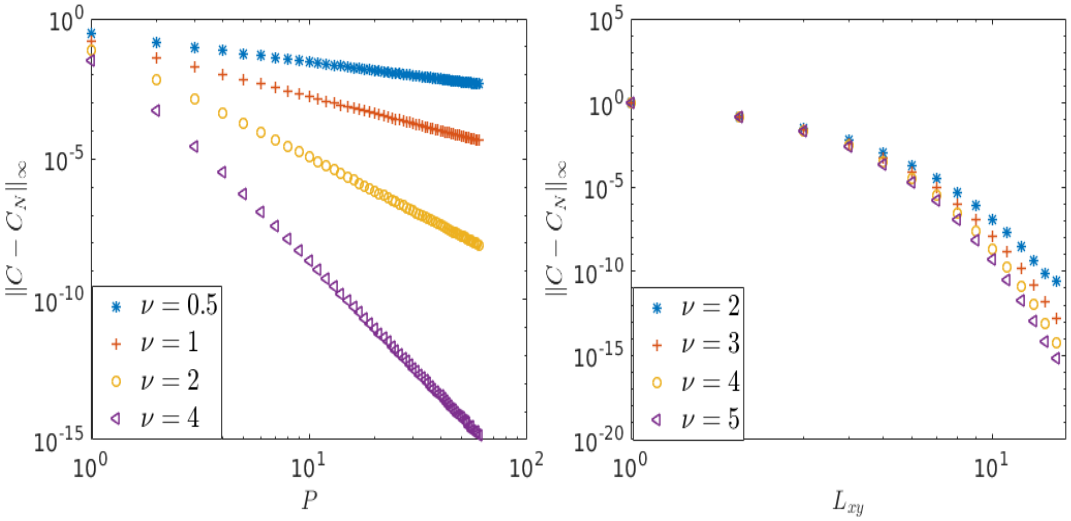

Figure 14: $\|C - C_N\|_\infty$ with respect to P. Figure 15: $\|C - C_N\|_\infty$ with respect to L.

Figure 14 illustrates the theoretical estimate bound of the weak error (on the covariance) $\|C - C_N\|_\infty := \max_{(x,y)\in D} |C(\|x - y\|_2) - C_N(\|x - y\|_2)|$ with respect to length of the frequencies domain $P = (1 : 1 : \frac{N}{L})$ in each direction. The discrete covariance matrix of the $2 - d$ discrete field G_N is given by,

$$C_N(\|x - y\|_2) = \frac{1}{4L_xL_y} \sum_{k=0}^{2N_x-1} \sum_{l=0}^{2N_y-1} \tilde{S}(p_k, p_l) e^{2i\pi p_k x + p_l y},$$

where $\tilde{S}$ is the symmetry of S in two directions. As expected, figure shows that the error with respect to P is algebraic since the spectral density S decreases algebraically as p becomes large. Figure14 plots the error $\|C - C_N\|_\infty$ with respect of the length of a square domain where $L = (1 : 1 : 15)$. For each case of ν we take a large number of equidistant points $N = 10^3$ to hide the error due to the discretization (frequency domain truncation). As expected, figure shows that the error with respect to L is sup-geometric since the covariance function decreases exponentially at infinity.

6 Conclusion

We have discussed the convergence of the spectral method that will, under suitable assumptions of the smoothness, produce realizations of a stationary and possibly anisotropic random process with minimal cost, through the FFT algorithm. Further, The spectral simulation is seen as the Karhunen-Loève discretization of a Gaussian

random field defined by a truncated of the target covariance function. Thus, we provide upper bounds of the convergence (in the weak and strong norm) of the spectral method. Both estimates show the efficiency of the method for smooth random field and defined by a regular spectral density function. For such random fields, the spectral representation discretization gives clearly accurate simulations regarding the methods based on the matrix decomposition. In particular, the circulant embedding approach for a model with covariance matrix which reaches the positivity for large spatial length or with truncation, while the spectral simulation method being considerably easier to implement and having a much lower computational. In contrast, when the Gaussian random field is rough, the method is not accurate because the roughness forces the discretization of the field on adequate large grid before to extract the desired simulation. The roughness of the spectral density forces the simulation on a suitable large length of spatial domain yielding to an additional computational effort.

References

[1] Robert J. Adler *The Geometry of Random Fields*, Classics in Applids Mathematics, SIAM 1981.

[2] A. Beaudoin, J.-R. de Dreuzy, J. Erhel and G. Pichot *Convergence analysis of macro spreading in 3D heterogeneous porous media*, ESAIM Proceedings. December 2013, Vol. 41, p. 59-76.

[3] Bochner, S. *Harmonic Analysis and the Theory of Probability*, Berkeley and Los Angeles University of California Press, 1955.

[4] John P. Boyd. *Chebyshev and Fourier spectral methods* . Dover Publications Inc., Mineola, NY, second edition, 2001.

[5] Chilès, J.-P., and Delfiner, P, *Geostatistics: Modeling Spatial Uncertainty*, New York: Wiley (1999).

[6] Dietrich, C. et G. Newsam. *A fast and exact method for multidimensional Gaussian stochastic simulation.* Water Resour. Res., (8), 2861-2869, 1993.

[7] Dietrich, C. et G. Newsam. *Fast and exact simulation of stationary Gaussian processes throught circulant embedding of the covariance matrix.* SIAM J. SCI. COMPUT. Vol. 18, No. 4, pp. 1088-1107, July 1997.

[8] J. Erhel, Z. Mghazli, M. Oumouni *An adaptive sparse grid method for elliptic PDEs with stochastic coefficients.*

[9] I.G. Graham, F.Y. Kuo, D. Nuyens, R. Scheichl, I.H. Sloan*Quasi-Monte Carlo methods for elliptic PDEs with random coefficients and applications.* Journal of Computational Physics, 230 (2011) 3668-3694.

[10] I.G. Graham, F.Y. Kuo, D. Nuyens, R. ScheichlAnalysis of circulant embedding methods for sampling stationary random fields, arXiv:1710.00751v1[math.NA] 2 Oct 2017

[11] L. W. Gelhar. *Stochastic Subsurface Hydrology.* Engelwood Cliffs. 1993.

[12] M. Loève: *Probability Theory I,II*, fourth edition, in: Graduate Texts in Mathematics, vol. 45,46, Springer-Verlag, New York, 1977-1978.

[13] G. Lord, C. Powell, T. Shardlow, *An Introduction to Computational Stochastic PDEs*, Cambridge University Press, Cambridge, 2014.

[14] R.L. Naff, D.F. Haley, and E.A. Sudicky, *High-resolution Monte Carlo simulation of flow and conservative transport in heterogeneous porous media 1.* Methodology and flow results, Water Resour. Res., 34, 663-677, 1998.

[15] Mircea Grigoriu. *On the spectral representation method in simulation.* Probabilistic Engineering Mechanics 1993.

[16] M.Oumouni, F.Schoefs, B.Castanier. *Modeling time and spatial variability of degradation through gamma processes for structural reliability assessment.* Structural Safety, V 76, 2019, 162-173.

[17] Shinozuka, M. and C.-M. Jan. *Digital simulation of random processus and its applications.* Journal of Sound and Vibration 1972 25 (l), 111-128

[18] Shinozuka, M. et G. Deodatis. *Stochastic process models for earthquake ground motion.* Probabilistic Engineering Mechanics, 1988, Vol. 3, No. 3

[19] Shinozuka, M. et G. Deodatis. *Simulation of stochastic processes by spectral representation.* App. Mech. Rev., 44(4), 191-204, 1991.

[20] Papakonstantinou KG, Shinozuka M. *Probabilistic model for steel corrosion in reinforced concrete structures of large dimensions considering crack effects.* J Eng Struct; 57:306-326, 2013.

[21] Stewart M., Mullard JA. *Spatial time-dependent reliability analysis of corrosion damage and the timing of first repair for RC structures.* Eng Struct, 29:1457-64, 2007.

[22] Wood, A. T. A., and Chan, G. *Simulation of Stationary Gaussian Processes in* $[0, 1]^d$. Journal of Computational and Graphical Statistics, 3, 409-432, 1994.

[23] A.M. YAGLOM, *Correlation Theory of Stationary and Related Random Functions*, Springer-Verlag, New York, 1987.